ACADEMIC PRESS

Available online at www.sciencedirect.com

SCIENCE DIRECT®

DEVELOPMENTAL BIOLOGY

Developmental Biology 256 (2003) 317–330

www.elsevier.com/locate/ydbio

Hoxb13 mutations cause overgrowth of caudal spinal cord and tail vertebrae

Kyriakos D. Economides,[a,1] Lori Zeltser,[b] and Mario R. Capecchi[a,*]

[a] *Howard Hughes Medical Center, Department of Human Genetics, University of Utah, Salt Lake City, UT 84112, USA*
[b] *Columbia University, Center for Neurobiology and Behavior, New York, NY 10032, USA*

Received for publication 22 October 2002, revised 16 December 2002, accepted 18 December 2002

Abstract

To address the expression and function of *Hoxb13*, the 5′ most *Hox* gene in the *HoxB* cluster, we have generated mice with loss-of-function and *β-galactosidase* reporter insertion alleles of this gene. Mice homozygous for *Hoxb13* loss-of-function mutations show overgrowth in all major structures derived from the tail bud, including the developing secondary neural tube (SNT), the caudal spinal ganglia, and the caudal vertebrae. Using the *β*-galactosidase reporter allele of *Hoxb13*, also a loss-of-function allele, we found that the expression patterns of *Hoxb13* in the developing spinal cord and caudal mesoderm are closely associated with overgrowth phenotypes in the tails of homozygous mutant animals. These phenotypes can be explained by the observed increased cell proliferation and decreased levels of apoptosis within the tail of homozygous mutant mice. This analysis of *Hoxb13* function suggests that this 5′ *Hox* gene may act as an inhibitor of neuronal cell proliferation, an activator of apoptotic pathways in the SNT, and as a general repressor of growth in the caudal vertebrae.

Keywords: *Hoxb* genes; *Hoxb13*; Secondary neurulation; Axial skeleton; Tail; Apoptosis; Proliferation

Introduction

The 39 vertebrate *Hox* genes are involved in patterning numerous axes and subaxes in the developing mouse. Numerous functions of *Hox* genes have been identified by gene-targeted mutagenesis in mice. A common theme to many of these analyses is the loss or reduction of structures, which include the axial–skeletal vertebrae (Condie and Capecchi, 1993; Favier et al., 1996; Fromental-Ramain et al., 1996; Ramirez-Solis et al., 1993; van den Akker et al., 2001), limb skeletal elements (Davis et al., 1995; Dolle et al., 1993), neural structures (Goddard et al., 1996; Studer et al., 1994, 1998), or internal organs (Chisaka and Capecchi, 1991; Patterson et al., 2001; Podlasek et al., 1997; Wellik et al., 2002). Some of the defects observed in mice with *Hox* loss-of-function mutations can be understood in the context of anterior homeotic transformations, where posterior genetic programs fail to be expressed due to the disruption of the posterior *Hox* gene (Bachiller et al., 1994; Duboule and Morata, 1994; Favier et al., 1995; Lufkin et al., 1992; Medina-Martinez et al., 2000).

Hoxb13 is the most 5′ gene in the *HoxB* cluster, and it is expressed, predictably, in the most posterior regions of the developing embryo. The expression pattern has been characterized until day 12.5 and is limited to the caudal extent of the spinal cord and tail bud, and the urogenital sinus (Zeltser et al., 1996). The expression of *Hoxb13* nicely coincides in a time with the dynamic changes associated with the formation of the secondary neural tube (SNT) and tail (Gofflot et al., 1997).

The caudal spinal cord and neural structures are derived from secondary neural tube, which is formed by secondary neurulation. Secondary neurulation begins after the posterior neuropore from primary neurulation has closed and is a process that is distinct from primary neurulation (Criley,

* Corresponding author.
E-mail address: mario.capecchi@genetics.utah.edu (M.R. Capecchi).
[1] Present address: Center for Advanced Biotechnology and Medicine, UMDNJ-Robert Wood Johnson Medical School, Piscataway, NJ 08854.

0012-1606/03/$ – see front matter © 2003 Elsevier Science (USA). All rights reserved.
doi:10.1016/S0012-1606(02)00137-9

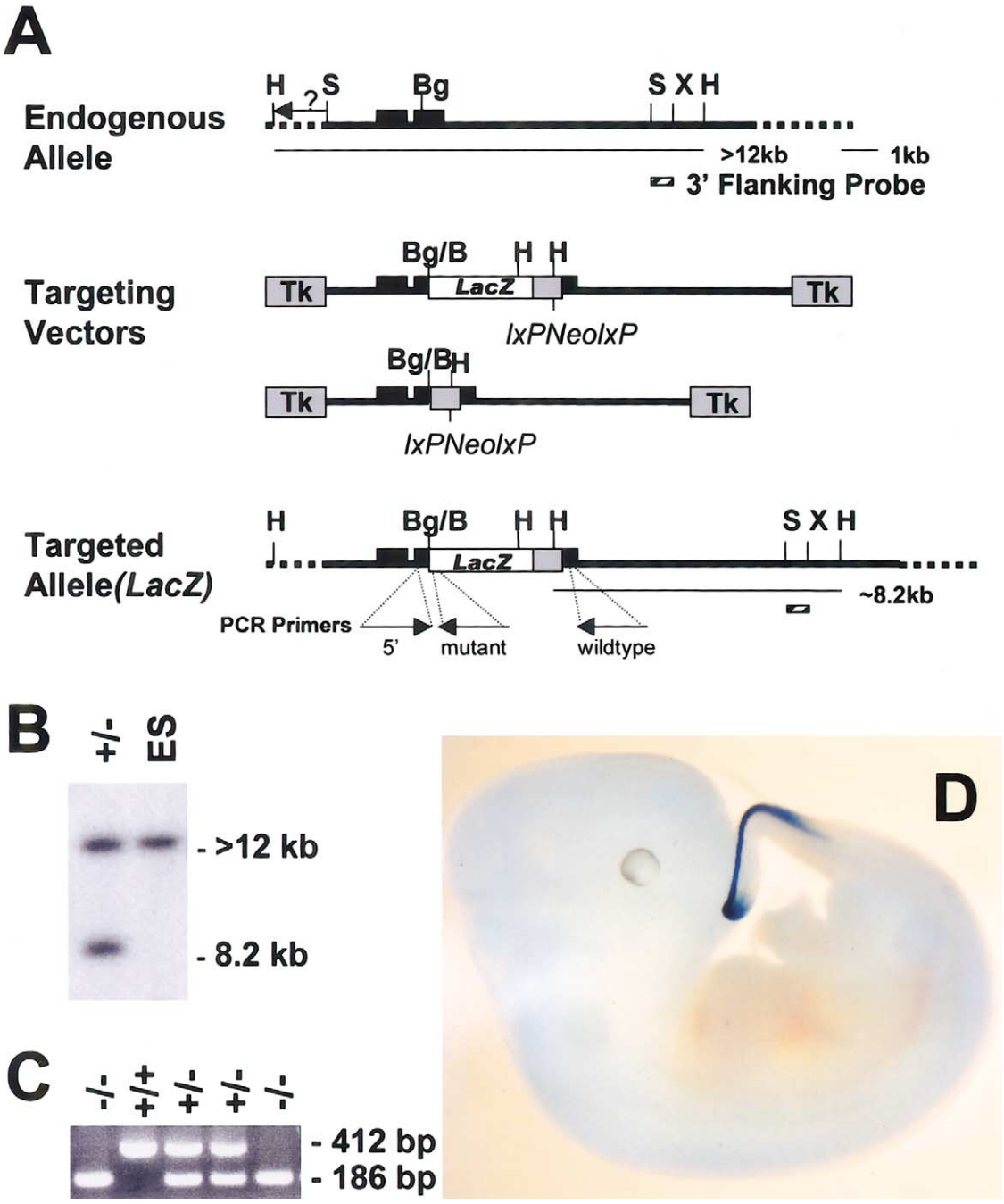

Fig. 1. Targeting strategy for disruption of the Hoxb13 locus. Schematic representation of the *Hoxb13* genomic locus, the two targeting vectors, and an example of the *hoxb13*^{lacZneo} targeted allele (A). Exons 1 and 2 of *Hoxb13* are represented by black boxes. *Neo*^{R} is represented by a gray box and *lac*Z and *Tk* genes are as labeled. The 3′ probe used for the initial screen is shown as a box with diagonal lines. *Neo*^{R} was subsequently removed by microinjection with Cre (for the *Hoxb13*^{lacZ} allele) or by mating with deletor Cre mouse (for the *Hoxb13*^{neo} allele). Example from a Southern blot analysis using the 3′ probe (0.7-kb *Sal*I/*Xba*I fragment) to identify targeted recombinants. ES cell DNAs were digested with *Hin*dIII (B). The endogenous allele produces a band that is larger than 12 kb, while introduction of a *Hin*dIII site from the *Neo*^{R} gene produces a mutant 8.2-kb band. PCR analysis of *Hoxb13*^{lacZ} mice. Genotype is determined by the resolution of a 186-bp band for the mutant allele and a 412-bp band for the endogenous allele (C). Initial assays were compared to Southern analyses to confirm the reliability of the PCR assay. X-gal staining of an heterozygous 11 day embryo (D). The staining pattern is consistent with previously reported in situ RNA hybridization data. Lxp, LoxP; Tk, thymidine kinase; B, *Bam*HI; Bg, *Bgl*II; H, *Hin*dIII; S, *Sal*I; X, *Xba*I.

1969; Schoenwolf, 1978). Whereas primary neurulation forms the primary neural tube (PNT) by folding of the developing neural plate, secondary neurulation forms the secondary neural tube by the differentiation of cells in the developing tail bud into a medullary cord, followed by cavitation of the cord to form a central canal (Schoenwolf, 1984; Schoenwolf and Delongo, 1980). The cells of the cavitated cord fuse and become continuous with the primary

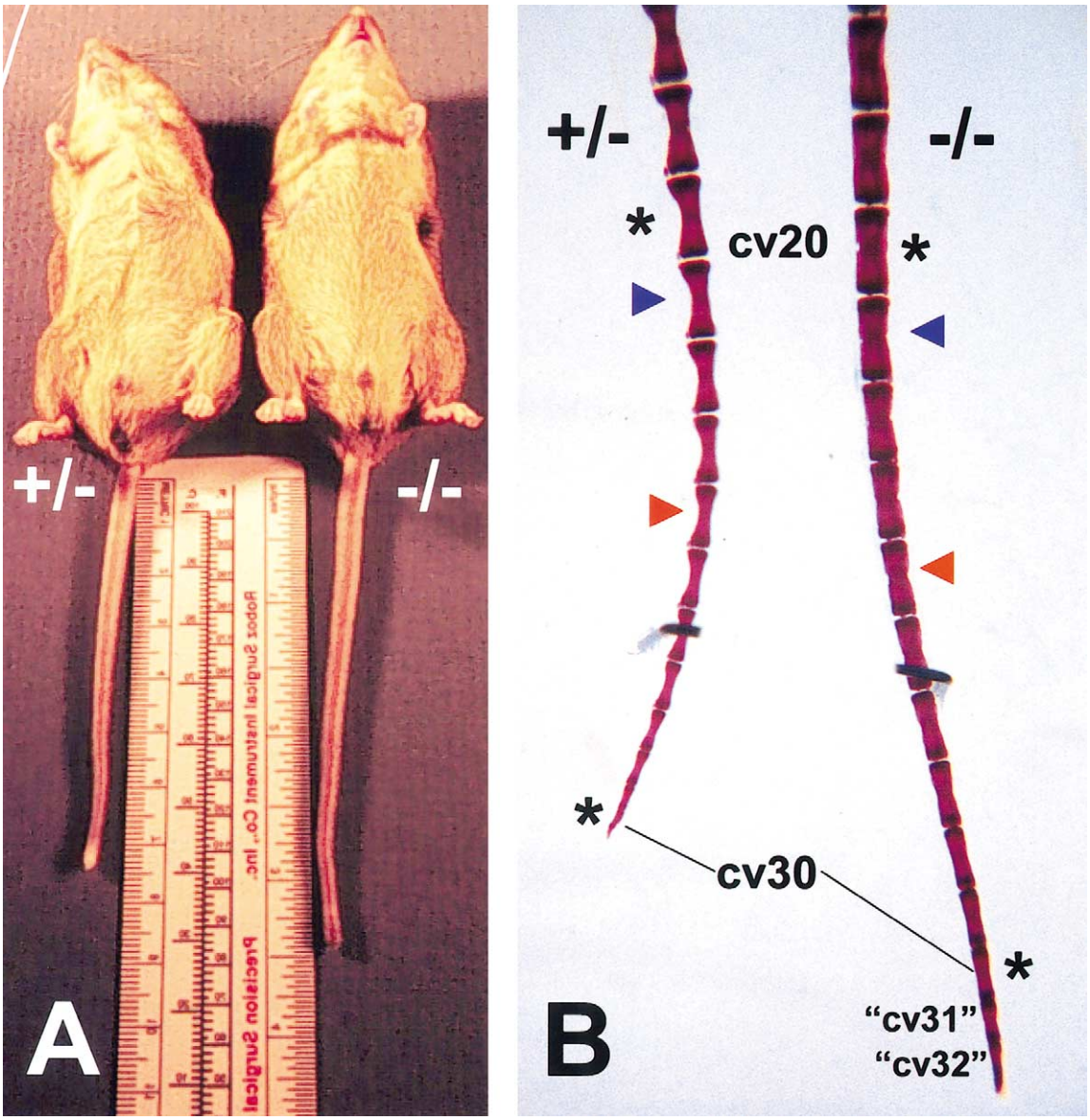

Fig. 2. Skeletal phenotype. *Hoxb13* heterozygote (left) and mutant (right) adults. Mutant mice have longer and slightly thicker tails (typically ~1 cm longer than heterozygotes or wild-type) (A). Close-up of the caudal-most vertebrae showing that in heterozygotes, the last 10 vertebrae taper off in length and width, and display a "bowtie" appearance (compare change in size from cv21 (blue arrowhead) to cv24 (red arrowhead) in heterozygote and mutant) (B). Individual mutant vertebrae are longer, thicker, and "barrel-shaped." cv, caudal vertebrae; asterisks mark positions of caudal vertebrae 20 and 30 in skeleton preparations.

neural tube. Tail bud outgrowth is a process similar to limb outgrowth, where a ventral ectodermal ridge (VER) has a similar function as the apical ectodermal ridge (AER) on the fates of mesenchymal cells within the tail bud (Goldman et al., 2000). The caudal neural tube, the caudal somites, and the neural crest derived caudal spinal ganglia are all derived from the tail bud. This process is well conserved in vertebrates regardless of whether or not the final adult form has a tail, but little is known about the genes involved in determining the final length and pattern of the adult tail (de Santa Barbara and Roberts, 2002).

To determine the role of *Hoxb13* in tail and caudal spinal cord development, we have generated loss-of-function alleles for *Hoxb13* by gene targeting. In this study, we describe overgrowth defects in the development of the caudal axial skeleton, caudal spinal cord, and neural crest derived spinal ganglia of *Hoxb13* homozygous mutants. While many *Hox* mutations result in loss of structures, very few *Hox* mutations have been identified where there is an increase in size or number of developing structures (Godwin and Capecchi, 1998; Stadler et al., 2001; Zakany et al., 1997), and no loss-of-function mutations have been identified that cause overgrowth of neural structures. The normal role *Hoxb13* in patterning the most caudal aspect of the mouse appears to be the repression of growth and activation of programmed cell death, thereby bringing finality to the developmental program.

Materials and methods

Generation of Hoxb13 mutant mice

A 13-kb genomic clone containing both exons of *Hoxb13* was obtained from a 129/Sv library in λFixII. A 9-kb *Sal*I fragment was subcloned into the *Xho*I sites of λDASH2Tk, a cloning phage containing Tk1 genes. An 1.7-kb internal *Xho*I fragment contained in the second exon and homeodomain of *Hoxb13* was also subcloned into a modified pSP72 cloning vector (Stratagene). A *Bam*HI/*Bgl*II fragment encoding β-galactosidase and a polyadenylation signal was cloned into the *Bgl*II site of the second exon, interrupting the gene at the 33rd amino acid residue of the homeodomain and placed in-frame with the aid of a custom linker (5′-GATCCGAGATCTCG-3′). A *Bgl*II fragment containing a loxP-flanked MC1 promoter driven Neo^R cassette was cloned into the *Bgl*II site downstream of the β-galactosidase reporter. For the knockout-only allele, the *Bgl*II Neo^R cassette was cloned into the genomic *Hoxb13 Bgl*II site to create a loss-of-function mutant allele for *Hoxb13* without a β-galactosidase reporter. In both lines, mice heterozygous for a mutant allele were bred to the Rajewsky Cre-deletor mouse line (Schwenk et al., 1995) to remove the Neo^R cassette. Removal of the Neo^R cassette in the knockout-only allele leaves a loxP site after the 33rd amino acid of the homeodomain and introduces a stop codon.

Genotype analysis

Cell lines and mice were screened by Southern blots using a 0.7-kb *Sal*I/*Xba*I 3′ flanking probe on a *Hin*dIII digest. The mutant allele is detected as an 8.2-kb *Hin*dIII fragment due to the addition of a *Hin*dIII site from the Neo^R cassette. Subsequently, PCR primers were created to detect the wild-type gene (sense 5′-AGGCCGCAAAAAACG-CATTCCC-3′; antisense 5′-AGGTTCTTCAGAACCGT-GATGGA-3′) or mutant allele (antisense 5′-CGCGCTC-GAGATGTGCTGCAAGGCGATTAA-3′). The wild-type gene is detected as a 412-bp PCR product, while the β-galactosidase fusion allele is detected as a 186-bp product.

Skeleton preparations

Animals were sacrificed by CO_2 asphyxiation and skin and viscera were removed. Skeletons were stained with alizarin red as previously described (Selby, 1987).

X-Gal staining of embryos

Embryos were stained for β-galactosidase activity with X-gal as previously described (Mansour et al., 1993). Briefly, embryos were fixed in 2% formaldehyde in 0.1 M PIPES buffer (pH 6.9), 2 mM $MgCl_2$, 1.25 mM EGTA pH 8.0 (from 10 min to 2 h based on age), washed three times in PBS/1 mM $MgCl_2$, and stained in 5 mM $K_3Fe(CN)_6$, $K_4Fe(CN)_6$, 1 mM $MgCl_2$, 0.01% sodium deoxycholate, 0.02% Nonidet P-40 (Sigma) in PBS pH 7.2 overnight at 30°C. Embryos were postfixed in 4% formaldehyde, washed, photographed, dehydrated, and embedded in paraffin or prepared for whole-mount immunohistochemistry as described below.

Whole-mount immunohistochemistry

Embryos were fixed in 4% formaldehyde for 2 h to overnight depending on age, rinsed three times in PBS, dehydrated through a MeOH series, and bleached overnight in 4:1:1 MeOH: H_2O_2 (30%):DMSO. Embryos were then rehydrated (50% MeOH then PBS), blocked two times, 1 h each in PBS + 2% milk + 0.5% Triton X-100 (Sigma). Primary Tuj1 monoclonal antibody (Covance) was added at 1:500 dilution and rocked overnight at 4°C. Embryos were washed five times, 1 h each and secondary peroxidase conjugated anti-mouse (Vector Labs) was added at 1:200 dilution overnight. Embryos were washed and developed using DAB substrate and cleared by a graded glycerol series or by dehydration followed by treatment with benzyl alcohol: benzyl benzoate 1:1.

TUNEL and pHH3 immunohistochemistry

Embryos were fixed in 4% formaldehyde (30 min to 2 h depending on age), rinsed three times in PBS, and stepped through a sucrose/PBS gradient (10, 20, 30% sucrose). Embryos were transferred to OCT, cryosectioned (10 μm), and mounted on superfrost (VWR) glass slides. Slides were washed with PBS, preincubated with PBS + 3% goat serum, and incubated with rabbit-polyclonal anti-phosphohistone H3 (pHH3; Upstate Biotechnology) (1:1000) and Tuj1 (1:1000) (Covance) overnight. Slides were then washed and incubated with secondary antibodies Cy5-conjugated anti-mouse, fluorescein-conjugated anti-rabbit IgG (Molecular Probes) in a mixture containing one-half of the manufacturer's recommendation of TUNEL buffer and enzyme (Roche).

Results

Generation of Hoxb13 mutant mice and genotype analysis

Four mutant alleles of *Hoxb13*, $Hoxb13^{lacZneo}$, $Hoxb13^{lacZ}$, $Hoxb13^{neo}$, and $Hoxb13^{lxp}$ were generated with two targeting vectors (Fig. 1A). In both targeting strategies a cassette was inserted into the second exon of *Hoxb13*, disrupting the homeodomain at the position of the 33rd amino acid. For the $Hoxb13^{lacZ}$ allele, a *Lac*Z gene followed by a polyadenylation signal sequence and loxP flanked Neo^R gene was inserted in-frame into the *Hoxb13* sequence. For the $Hoxb13^{neo}$ allele a loxP flanked Neo^R was inserted directly into *Hoxb13*. Targeting vectors were elec-

troporated into embryonic stem (ES) cells and positive–negative selection was used to enrich for cells containing the *Hoxb13*-targeted recombination (Mansour et al., 1988). Using a 3′ flanking probe for Southern blot analysis, cell lines were identified that contained the proper *Hoxb13^{lacZ}* allele or the *Hoxb13^{neo}* allele (Fig. 1B). Internal probes were used to rule out potential multiple integrations of the targeting vector and/or microdeletions at the target locus (data not shown). Two independent cell lines for each of the alleles were used to generate chimeric mice capable of transmitting the mutant alleles to their offspring. A PCR assay was developed to facilitate genotyping of subsequent progeny (Fig. 1C). Mice containing the *Hoxb13^{lacZ}* allele that were stained with X-Gal showed identical expression patterns (Fig. 1D) to that reported in previous work by in situ hybridization with an antisense *Hoxb13* probe (Zeltser et al., 1996). The mutant phenotypes of mice homozygous for each of the four *Hoxb13* alleles were indistinguishable. Most of the studies described used embryos or mice carrying the *Hoxb13^{lacZ}* or *Hoxb13^{lxp}* mutant alleles. Crossing mice harboring the *Neo^{R}* alleles to a Cre-deletor strain (Schwenk et al., 1995) generated these alleles. For the *Hoxb13^{lxp}* mutant allele a LoxP site remains and places a stop codon immediately after the 33rd amino acid of the homeodomain.

Skeletal phenotypes are detected in Hoxb13 mutants

Viability and fertility were normal for both heterozygous and homozygous mutants. A striking phenotypic difference is the morphology of the tail where tails from homozygous mutants within the same litter were longer and thicker. When we compared 23 mice from three different litters, all mice that had tails >9 cm were later found to be mutant homozygotes ($N = 10$). Overall, genotype can be predicted based on an approximately 1 cm greater length in the tail of a mutant over that of a heterozygote within a given litter (Fig. 2A). In addition to a longer tail, the vertebrae of the mutants are thickened relative to the heterozygotes. This is especially evident in the more caudal vertebrae where in heterozygotes they taper and individual vertebrae assume a "bowtie" appearance, while in homozygous mutants, vertebrae are thicker and more "barrel" shaped (Fig. 2B). Gross anatomical defects were not observed in the sacral or anterior caudal vertebrae as seen with *Hoxc13* homozygous mutants (Godwin and Capecchi, 1998), except for a greater distance between the bifid spinous processes of caudal vertebra 1–6, which is described later. No differences were noted between heterozygous and wild-type mice.

Hoxb13 expression and mutant phenotypes in the secondary neural tube

To further define the expression of *Hoxb13*, and to identify potential defects in *Hoxb13* expressing cells during embryogenesis, we stained embryos with X-gal during various stages from day 10.5 to day 17.5 of gestation (E10.5–E17.5). No abnormalities were detected through E11.5. At E12.5, however, the homozygous mutant spinal cords were clearly wider and longer than heterozygote spinal cords. Additionally, a dorsal flexure of the tail is evident in all homozygous mutants, as well as strong staining of the caudal dorsal root ganglia (DRGs) (Fig. 3A and B). Expression of *Hoxb13* was limited to the neural tube and the caudal extremity of the tail bud through E13 (Fig. 3C and D). By E14.5, in addition to expression in the neural tube, the caudal one-third of the tail shows strong staining throughout the tail bud mesenchyme. At this stage in development the difference between the length of the heterozygote and mutant spinal cords is very noticeable (Fig. 3E and F). A longer and thicker spinal cord at the caudal extremity was apparent with any combination of two mutant *Hoxb13* alleles, including *Hoxb13^{lxp}/Hoxb13^{lxp}*, indicating that this phenotype was not due to the presence of β-galactosidase or *Neo^{R}*. No differences were detected between heterozygous and wild-type mice and in subsequent experiments heterozygotes were used as controls. Since the *Hoxb13^{lacZ}* allows reproducible staining of the caudal spinal cord, all subsequent experiments were carried out using the *Hoxb13^{lacZ}* allele.

At E15.5, a spinal cord was absent from the region of the tail expressing *Hoxb13* in heterozygotes, while a spinal cord and an aberrant mass of neural tissue at the very caudal extremity was evident in homozygous mutants (Figs. 3G–J). The caudal extremity of the spinal cord, termed the conus medullaris, was located more posteriorly in mutant homozygotes relative to heterozygotes. When we dissected out the neural tissue, we confirmed that that the cord was actually thickened through the entire length of *Hoxb13* expression domain (Fig. 3K and L). In addition to the β-galactosidase expression in the SNT and caudal mesenchyme, strong activity was observed in four parallel domains that run the length of the tail (Fig. 3I and J). Further analysis demonstrated that these four expression domains are closely associated, but not superimposed, with the four large segmental nerve tracts (white arrowheads, Fig. 3M and N). Transverse sections through homozygous mutant neural tubes of X-gal stained embryos, followed by immunohistochemistry with a neural specific Tuj1 antibody (Moody et al., 1996), showed increased numbers of Tuj1-positive cells arranged in six to eight layers (Fig. 3P), while heterozygote control neural tubes always contained two layers of cells, one inner undifferentiated ventricular layer, and one outer, postmitotic Tuj1-positive layer (Fig. 3O). Additionally, there was strong expression of the β-galactosidase reporter in the dorsal most region of homozygous mutant neural tubes, while it is lacking in the heterozygote, indicating that these cells are normally lost (black arrowheads, Fig. 3O and P). Two copies of the *Lac*Z reporter versus one copy do not explain these differences, since the *Hoxb13^{lacZ}/Hoxb13^{lacZ}* and *Hoxb13^{lacZ}/Hoxb13^{laxP}* animals displayed identical phenotypes. In addition to the tail expression, *Hoxb13^{lacZ}* was detected in the developing urogenital sinus, but no

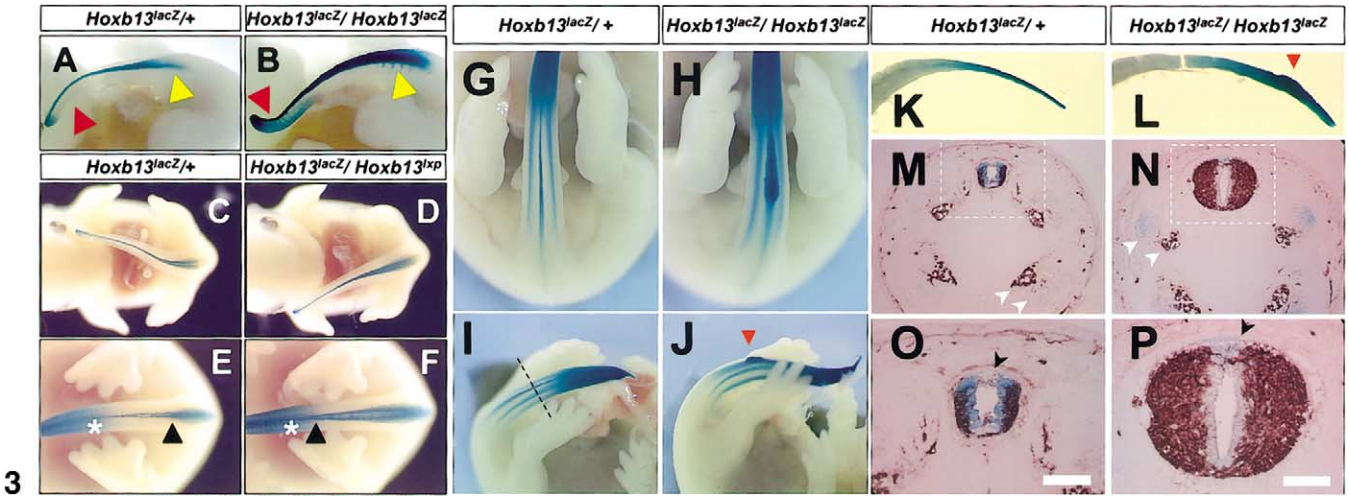

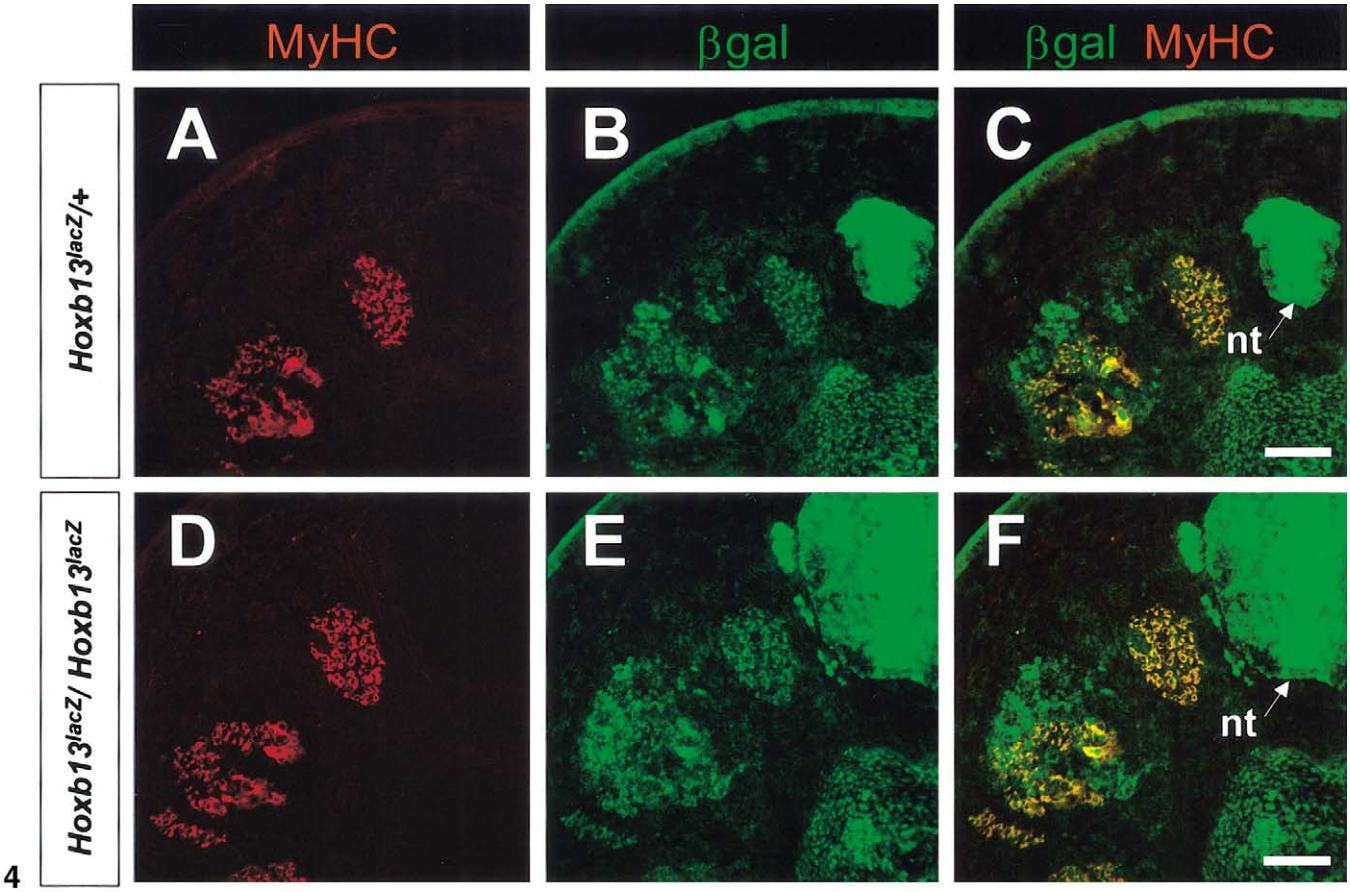

Fig. 3. Analysis of *Hoxb13* tail expression and phenotypes at day 12.5 to 15.5. Expression of *Hoxb13* was followed in heterozygotes and mutants using the β-galactosidase reporter. At day 12.5 strong expression of the reporter is seen in the ectopic spinal ganglia (yellow arrowheads, A, B) and there is a dorsal flexure in homozygous mutants (red arrow, A, B). Day 13 and 14.5 homozygous mutant embryos are $Hoxb13^{lacZ}/Hoxb13^{lxp}$ animals to rule out the possibility that an extra copy of β-galactosidase is contributing to the phenotype. Day 13 embryos show a phenotype in the neural tube, but expression has not turned on in the mesoderm at this point (C, D). By day 14.5 the differences in the developing spinal cord length are profound (E, F, black arrows) and expression in the mesoderm is evident (E, F, white asterisk). Dorsal (G, H) and lateral (I, J) views of day 15.5 embryos stained with X-gal show strong staining in the neural tube, caudal mesoderm, and in four parallel domains along the tail. *Hoxb13* homozygous mutants have a developing *conus medullaris* far more caudal than in heterozygotes. Removal of the SNT in heterozygotes and mutants shows that the spinal cord is thickened along the entire length in mutants (K, L) and a mass of aberrant neural cells is seen in the caudal extremity of the mutant cord (red arrowheads in J and L). Paraffin sections of X-gal-stained embryos followed by Tuj1 immunohistochemistry at the level of the dashed line in I and red arrowhead in J reveal that the four parallel domains (blue) do not align with the four segmental nerves (dark brown) (white arrowheads in M and N). Closer inspection reveals only two cell layers in heterozygote, a ventricular undifferentiated cell layer and a Tuj1 positive layer, while mutants have a ventricular layer and multiple Tuj1-positive layers (O, P). Also note the absence of X-gal positive staining in the dorsal neural tube in the heterozygote, while in the mutant it is the darkest staining for X-gal (compare black arrowheads in O and P). Scale bar = 50 μm.

Fig. 4. Myosin heavy chain and βgal immunohistochemistry at day 15.5. The dark X-gal staining in four tracts in Fig. 5 is explained by expression of the β-galactosidase reporter in four parallel muscle tracts. Myosin heavy chain (A, D) and β-galactosidase (B, E) antibodies colocalize in the muscle. Expression of β-galactosidase in the muscle is qualitatively lower than in the neural tube (C, F). The expression domains of *Hoxb13* are slightly broader than MyHC, suggesting that *Hoxb13* expression slightly precedes muscle development. nt = neural tube. Scale bar = 50 μm.

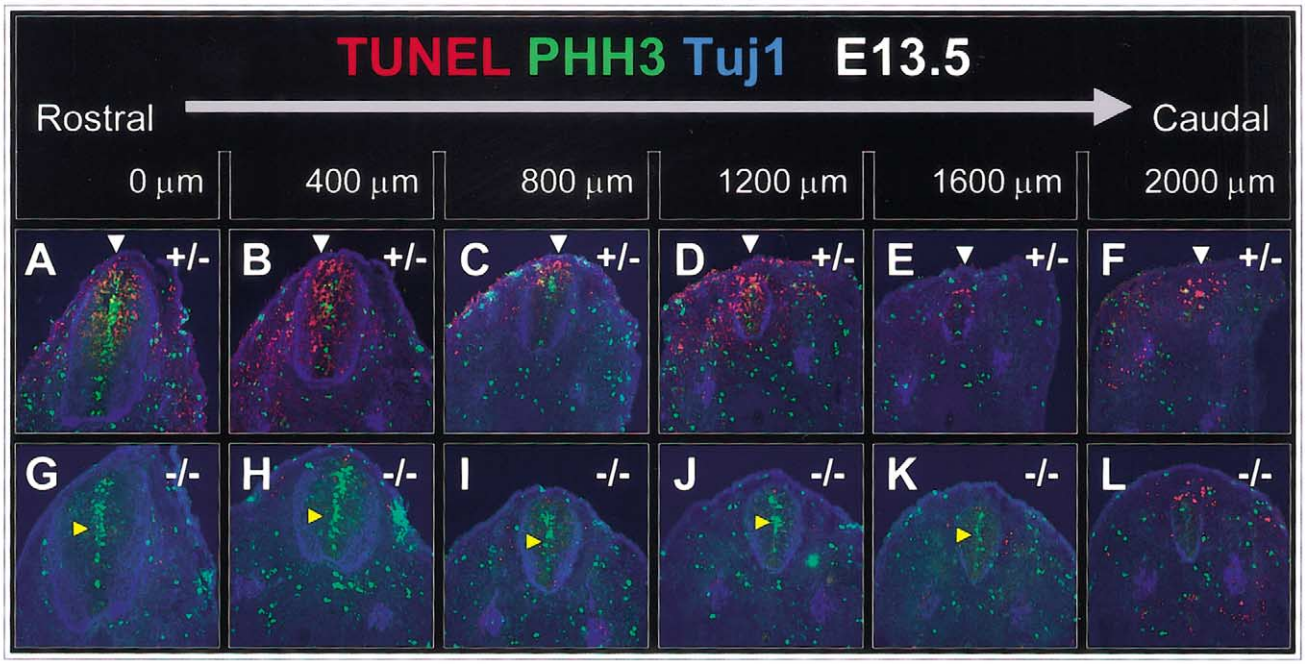

5

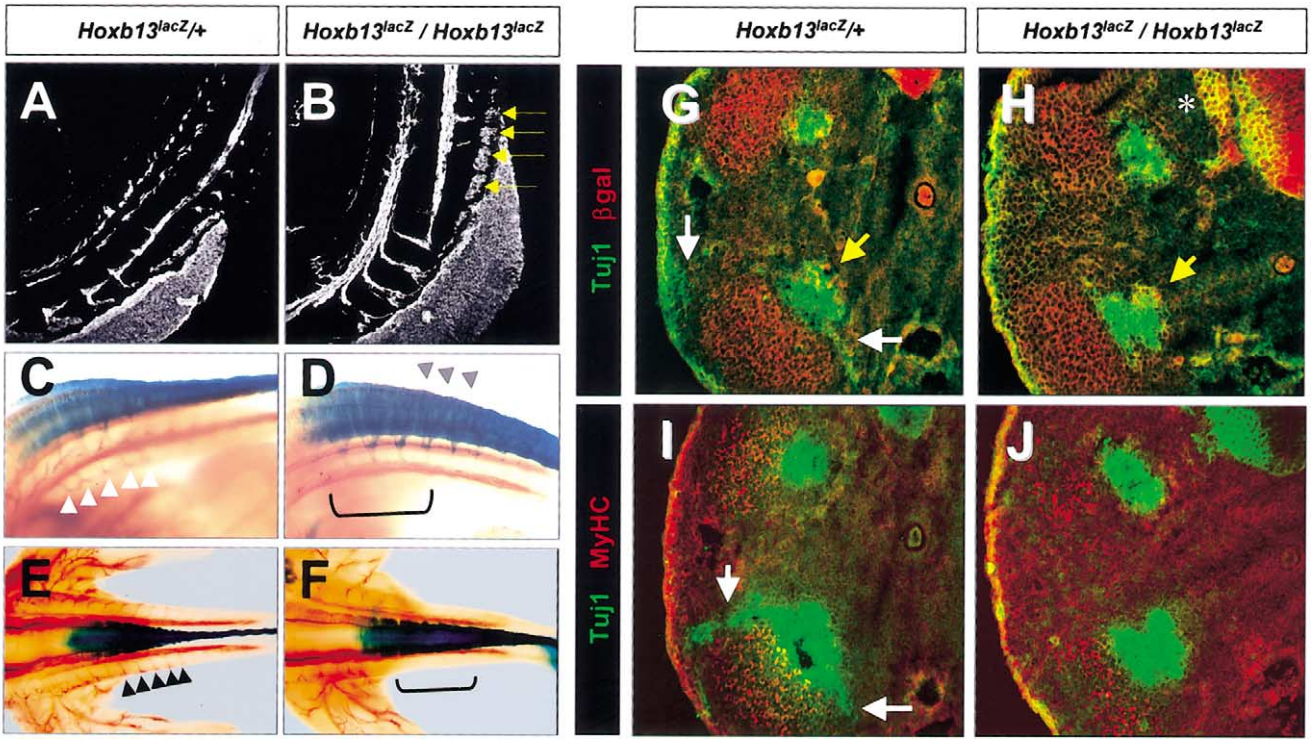

6

Fig. 5. pHH3 and Tuj1 immunohistochemistry followed by TUNEL. Day 13.5 *hoxb13*$^{lacZ/+}$ (A–F) and *hoxb13*$^{lacZ/lacZ}$ (G–L) embryos were cryosectioned and stained using antibodies for pHH3 (green channel) and Tuj1 (blue channel). TUNEL was performed concurrently with secondary (fluorophore-conjugated) antibody incubation (red channel). The 0-μm point is determined by the position of the genital tubercule and hindlimbs (not shown). Serial sections reveal a significant lack of apoptosis in the homozygous mutant neural tubes even in very rostral sections (white arrowhead, A, G). Mitosis is comparable at this level but drops off dramatically in more caudal levels (compare B–E with H–K). pHH3 staining is strong throughout most levels (yellow arrowheads), finally diminishing at about 2 mm caudal. Note that apoptosis appears normal at the most caudal sections (F, L).

Fig. 6. *Hoxb13* mutants have ectopic spinal ganglia and aberrant nerve tracts. Tuj1 antibody staining of sagittal sections through day 13.5 embryo spinal cords at the level of the most caudal DRGs (A, B). Mutants display extra 3–4 spinal ganglia (yellow arrows in B). These can also be seen in Tuj1 whole-mount immunohistochemistry (C–F) of X-gal-stained embryos (gray arrowheads in D). Although there are more axons from DRGs fasciculating with the segmental nerves, there are fewer defasciculating in homozygous mutants (compare mutants D and F (brackets) to C (white arrowheads) and E (black arrowheads)). In sections through day 13.5 tails (G–J), β-galactosidase (red) and Tuj1 (green) immunohistochemistry reveals branches that are evident leaving the ventral segmental nerve tract to the periphery (white arrows G and I) but are absent in mutants (H and J). β-Galactosidase is also detected in a subset of nerve tracts in the segmental nerves (yellow arrows in G and H). Myosin heavy chain-positive cells (red) are next to the segmental nerves in adjacent sections (I, J). Also note the β-galactosidase expressing ectopic DRG that is evident in the Hoxb13 homozygous mutant (asterisk in H).

morphological defects were identified within tissue in *Hoxb13* mutant homozygotes during development and these mutant male mice are fertile (data not shown). However, a very specific defect was identified in these mutant mice involving the secretory function of the ventral prostate (Economides and Capecchi, unpublished results).

Hoxb13 is expressed in muscle progenitors

The morphology and position of the four X-gal-stained tracts parallel to the segmental nerves suggested that *Hoxb13* is expressed in muscle as well as in the SNT. We exploited the β-galactosidase reporter using antibodies against β-galactosidase (βgal) and myosin heavy chain (MyHC) for double-labeling immunohistochemistry. βgal colocalized (Fig. 4B and E) with MyHC (Fig. 4A and D) expression and also extended slightly beyond the MyHC expression domain (Fig. 4C and F). This suggests that *Hoxb13* is expressed earlier than myosin heavy chain. This was confirmed with double immunohistochemistry for βgal and myogenin, which showed that *Hoxb13* was also expressed in early muscle progenitors (data not shown). It was clear from the intensity of the staining that *Hoxb13* was expressed at lower levels in the muscle than in the neural tube (Fig. 4C and F). The earliest stage where β-galactosidase was detected in muscle by antibody staining was E13.5 (data not shown).

Hoxb13 coordinates cell death and cell proliferation

Programmed cell death has an important role in the normal process of degeneration of the secondary neural tube. To determine whether the extended spinal cord phenotype was due to overproliferation of neural progenitors in the SNT, a reduction in the normal process of programmed cell death, or both, we carried out an assay to evaluate apoptosis and mitosis. Frozen sections were incubated with an anti-phosphohistone H3 antibody to label mitotic cells, followed by TUNEL to detect apoptotic cells. From E11.5 to E12.5 no obvious differences in labeling were noted between controls and mutants (data not shown). At E13.5, however, differences in both cell proliferation and apoptosis were noted when comparing mutant homozygotes to heterozygotes (Fig. 5A–L). Transverse sections were taken using the level where the tail connects to the body wall in both heterozygotes and mutants as a starting point (Fig. 5A and D). At this level, SNTs looked very similar, and pHH3 staining appeared equal. TUNEL revealed that there was more apoptosis in heterozygotes compared to mutant homozygotes (Fig. 5A and G). In more posterior sections, there was a sharp decrease in cell proliferation in heterozygotes, while cell death is observed throughout the SNT (Fig. 5B–F). In homozygous mutants, cell proliferation was seen at nearly all levels through the SNT, while cell death is greatly reduced (Fig. 5H–L). These results were observed consistently in all E13.5 mutant embryos ($n = 4$ pairs). The ectopic spinal cords in homozygous mutant embryos up to E15.5 expressed pHH3 in the ventricular cell layers indicating that, even at this late stage, there is aberrant cell proliferation in the SNT (data not shown). These data suggest that *Hoxb13* is involved not only in regulating cell death in the caudal spinal cord, but also blocks proliferation of neuronal cells within the secondary neural tube.

Hoxb13 mutants have supernumerary DRGs and defective axon pathfinding

In addition to a caudally extended spinal cord, mice that are mutant for *Hoxb13* also have supernumerary spinal ganglia. These were seen in sagittal sections of E13 embryos stained with Tuj1 antibody (Fig. 6A and B) and in whole-mount X-Gal/Tuj1 staining of E13.5 embryos (Fig. 6C and D). *Hoxb13* is expressed in the normal caudal-most DRGs in heterozygotes (Fig. 6C). In homozygous mutants, there were three to four ectopic DRGs, which also expressed *Hoxb13*^{lacZ} (Fig. 6D, gray arrowheads). Axons from the caudal DRGs fasciculate with the four segmental nerves that run the length of the tail (Fig. 6C and D). Segmental nerves at this stage appeared thicker in the homozygous mutants and did not extend as far caudally as in their heterozygote littermates (Fig. 6E and F). Upon close inspection we saw that more processes entered the segmental nerves from ectopic DRGs, but there were fewer ventral and lateral processes defasciculating to innervate the peripheral tissues of the tail in homozygous mutants when compared to heterozygous animals (Fig. 6C–F). Lack of defasciculation in homozygous mutants was also detected in sections. Adjacent sections stained with Tuj1/βgal or Tuj1/MyHC show Hoxb13-positive processes fasciculating with the segmental nerves (Figs. 6G and H, yellow arrows), but lateral and ventral processes exiting the segmental nerves are observed only in heterozygotes (Fig. 6G and I, white arrows). Homozygous mutant mice have been tested for cold or hot sensitivity as well as for pressure, touch, and pain sensitivity and appear capable of sensing these stimuli; however, they reproducibly exhibit a less pronounced tail-flick response (data not shown). This implies that peripheral nerve innervation is not completely abolished in homozygous mutants, but is demonstrably reduced in these mice.

Spinal cord defects persist in newborns and adults

The principal *Hoxb13* mutant phenotype in the CNS, the caudally extended spinal cord, persists from birth into adulthood. In sagittal sections of the tail of newborn mice, the spinal cord with an intact central canal was apparent in mutant homozygotes, while in heterozygotes no spinal cord is observed and only the filum terminale can be seen (Fig. 7A and B). When we sectioned through tails at the level of caudal vertebra 3 in 16-week-old heterozygotes and homozygous mutants, the presence of spinal cord tissue could only be seen in the homozygous mutants (Fig. 7D). Closer

inspection revealed a structurally abnormal spinal cord complete with rudimentary DRGs. Common to both heterozygote and mutant homozygotes are two nerve tracts within the vertebral foramen, known as ventral ramii. However, the ventral ramii in the mutants were considerably larger in than the heterozygote controls (Fig. 7C and D). Ventral ramii have been followed through caudal vertebrae 4 and 5 in mutants but terminate shortly after entering caudal vertebra 4 in heterozygotes (data not shown). The mutant cord begins to diminish considerably by caudal vertebra 5. The vertebral foramena in more rostral vertebrae serve as a channel for the spinal cord to pass through. Foramena are evident in mice through all the sacral vertebrae, and through approximately caudal vertebra 6, despite the fact that these vertebrae do not surround a spinal cord at these caudal levels (our observations, data not shown). The foramena in more caudal vertebrae are a remnant of the prechondrogenic condensations that were laid down around the embryonic spinal cord, which later regresses due to differential growth between the spinal cord and vertebral column. When comparing caudal vertebrae 1 through 6 between heterozygote and homozygous mutant littermates, the mutant foramena are always larger and the bifid spinous processes are set farther apart. The aberrant spinal cord in mutants displaces developing structures during condensation of the vertebral processes. Staining for both muscle and neural tissue illustrates that the developing muscle bundles are pushed farther apart to accommodate a larger neural tube (Fig. 7E and F). A 50% increase in the distance between developing structures (Fig. 7G and H), for example, leads to a corresponding increase between vertebral features such as bifid spinous processes (Fig. 7I–L). The subtle defects in the shape of the caudal vertebrae, therefore, appear to be secondary to the primary defect—the larger secondary neural tube in homozygous mutants.

Discussion

Utilizing mice with a targeted disruption of *Hoxb13*, we have demonstrated that *Hoxb13* is essential for the normal development of the vertebrate tail. Using a *Hoxb13*^{lacZ} reporter allele, we detected expression of *Hoxb13* from E9.5 until E16.5. At E11.5 it was evident that homozygous mutant spinal cords were longer and thicker than normal. At E12.5 we detected a second wave of Hoxb13 expression in the mesoderm starting at the tip of the tail and extending through approximately the caudal one-third of the tail. Similar to the overgrowth defect observed in the SNT, we saw an overgrowth defect in vertebrae derived from the most caudal somites that corresponds to the second wave of Hoxb13 expression in the mesoderm and explains the longer overall tail length in homozygous mutant adults. Finally, we detected Hoxb13 expression in the caudal spinal ganglia. Therefore, it appears that Hoxb13 also controls rates of proliferation of the neural crest. In summary, *Hoxb13* affects the growth and patterning of all three major derivatives of the tail bud (summarized in Fig. 8).

Many classical mutants that affect tail length and patterning have been described. These classical mutations include *brachyury* (Wittman et al., 1972), *vestigial tail* (Gruneberg and Wickramaratne, 1974), *curly tail* (Gruneberg, 1963), and *Danforth's short-tail (sd).* A general property of all of these mutations is a shorter or truncated tail (Gruneberg, 1963) as opposed to a longer tail in *Hoxb13* mutants. *Danforth's short-tail,* for example, is a semidominant mutation characterized by degeneration of the notochord and apoptosis of epaxial myotome (Asakura and Tapscott, 1998). *Curly tail* and *vestigial tail* share some similarities with *Hoxb13* in that both of these mutations cause an initial overproliferation and/or misspecification of neural structures. In *curly tail,* for example, there is overproliferation of neuronal cell types within the tail bud of developing mice (Keller-Peck and Mullen, 1997; van Straaten and Copp, 2001).

Overproliferation of these neuronal cell types cause tail flexures similar to those seen in *Hoxb13* homozygous mutant embryos, and ultimately, prevent posterior neuropore closure and lead to spina bifida. Unlike *Hoxb13,* however, these events have been temporally and spatially linked to overproliferation during primary neurulation, rather than secondary neurulation (Copp and Brook, 1989; van Straaten et al., 1992). *Vestigial tail* mutations cause the formation of ectopic neural tubes and are described later.

Tail length in vertebrates is determined by two major factors. Early signaling events between the VER and the tail bud mesenchyme (TBM) begin around the time of posterior neuropore closure, which heralds the end of both primary neurulation and gastrulation. The tail bud initiates as a mass of undifferentiated mesenchyme followed shortly by formation of the VER, a ridge of signaling tissue that is similar in structure and function to the AER in limb development (Goldman et al., 2000). The developing tail bud gives rise to three major structures of the tail: the secondary neural tube, the caudal somites, and the neural crest derived caudal spinal ganglia (Schoenwolf, 1978; Schoenwolf et al., 1985).

The second factor that helps determine the length and patterning of the tail are events that quickly follow the initial outgrowth of the tail and involve the generation and degeneration of different tail components. The degeneration of caudal structures occurs by programmed cell death and is a major contributor to the final pattern of the developing tail (Nievelstein et al., 1993).

In mice, the spinal cord in the tail region is a transient structure. Shortly after posterior neuropore closure at around E9 of development, the secondary neural tube begins to form (Gofflot et al., 1997). At E10 to E10.5 a column of neurectodermal cells differentiate. At this stage, all 34–35 spinal ganglia have formed. By E12 nuclei within the SNT are aligned at two levels, a ventricular progenitor level and an outer differentiated level. Degeneration and differentiation of the SNT takes place starting at E12 and up to

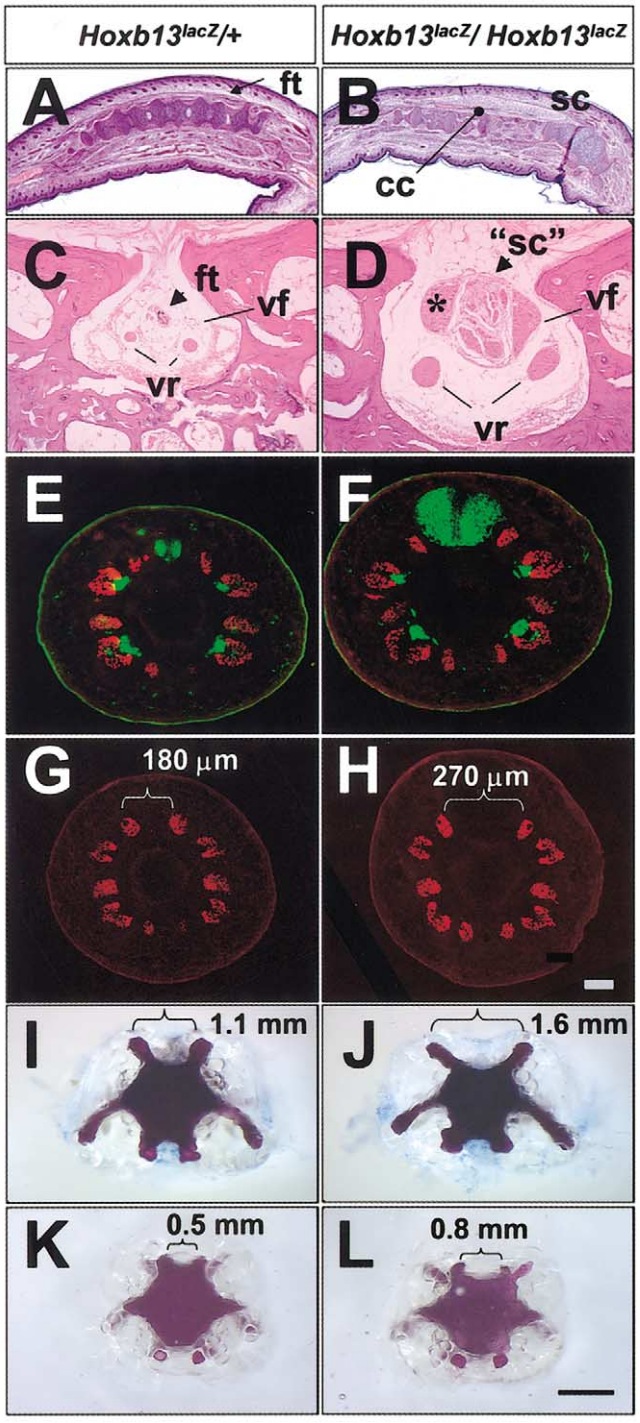

Fig. 7. The spinal cord phenotype persists through birth and adulthood. Hematoxylin and eosin staining of sagittal sections through the tail of newborn mice (A, B). The spinal cord is evident in mutant homozygotes (B) but not heterozygotes (A). The central canal is clearly visible within the spinal cord in mutant homozygotes but heterozygotes show evidence of only a filum terminale. Hematoxylin and eosin staining of transverse sections through adult caudal vertebra 3 in a heterozygote and homozygous mutant show that the vertebral foramen is larger and a spinal cord remnant is visible in the homozygous mutant (C, D). Within the vertebral foramen, the filum terminale is visible in the heterozygote, while an aberrant spinal cord is seen in the homozygous mutant, complete with rudimentary DRGs (asterisk). The ventral ramii are also enlarged in the homozygous mutant relative to the heterozygote. Rostral (E, F) and more caudal sections (G, H) through an area of a developing day 15.5 tail near the genital tubercule (rostral 1/3 of the tail): MyHC/Tuj1 double immunohistochemistry in heterozygote (E) and homozygous mutant (F) and MyHC only in heterozygote (G) and homozygous mutant (H). Note that the dorsal muscles are pushed apart in the mutants to accommodate a larger neural tube. An approximately 50% increase in the distance between developing structures causes a corresponding increase in the distance between superior bifid spinous processes (I, J) as well as the inferior bifid spinous processes (K, L) in adults. Shown are dissected alizarin red stained vertebrae- superior view of caudal vertebra 4 (I, J) and inferior view of caudal vertebra 5 (K, L). Scale bar in H (for E–H) is 100 μm. Scale bar in L (for I–L) is 1 mm. All figures are oriented so that dorsal is top, and ventral is bottom. cc, central canal; ft, filum terminale; sc, spinal cord; va, vertebral arch; vf, vertebral foramen; vr, ventral ramii.

E17. During this time apoptosis is observed along the entire length of SNT and a thin, fibrous layer in the rostral SNT differentiates to form a tissue continuous with the PNT called the filum terminale (Nievelstein et al., 1993). This tissue runs the length of the tail and serves as a continuation of the dura mater and pia mater that surround the spinal cord. The most caudal end of the remaining spinal cord is known as the conus medullaris. Differential growth between the spinal cord and the vertebral axial skeleton accounts for a final position of the spinal cord relative to vertebral bodies that is far more rostral in an adult vertebrate than in an embryo or newborn (O'Rahilly et al., 1990). For example, the caudal extent of the spinal cord is around T12 to L2 in adult humans, and L3 to L4 in adult mice and rats.

There are at least two possible explanations for the phenotypes seen in *Hoxb13* mutants. One possibility is that there is a defect in the early events of tail bud formation leading to the production of more precursors for the development of the tail. In *vestigial tail (vt)* mice, which carry a mutation in *Wnt3a* (Yamaguchi et al., 1999), ectopic neural tubes are formed at the expense of mesoderm and the tail rapidly degenerates (Shum et al., 1999; Takada et al., 1994). Because there is overabundance of neural tissue in the tails of *Hoxb13* homozygous mutants, *Wnt3a* expression was examined, but no differences were detected between *Hoxb13* homozygous mutants and controls (data not shown). This suggests that the phenotypes associated with *Hoxb13* mutations are not due to the early patterning events that are associated with *Wnt3a* expression.

A second possibility is that *Hoxb13* is required to coordinate proliferation and apoptosis during secondary neural tube formation and degeneration later in tail development. We believe that this is the more likely scenario for the following reasons: (1) The expression pattern of *Hoxb13* later in tail development is consistent with the later events that determine tail length; (2) In contrast to *vt* mutants, neural structures in the tail of *Hoxb13* homozygous mutants are not made at the expense of other tissue types (Yoshikawa et al., 1997), rather there appears to be overproliferation of cells everywhere that *Hoxb13* would normally be expressed; (3) The embryonic age at which differences are

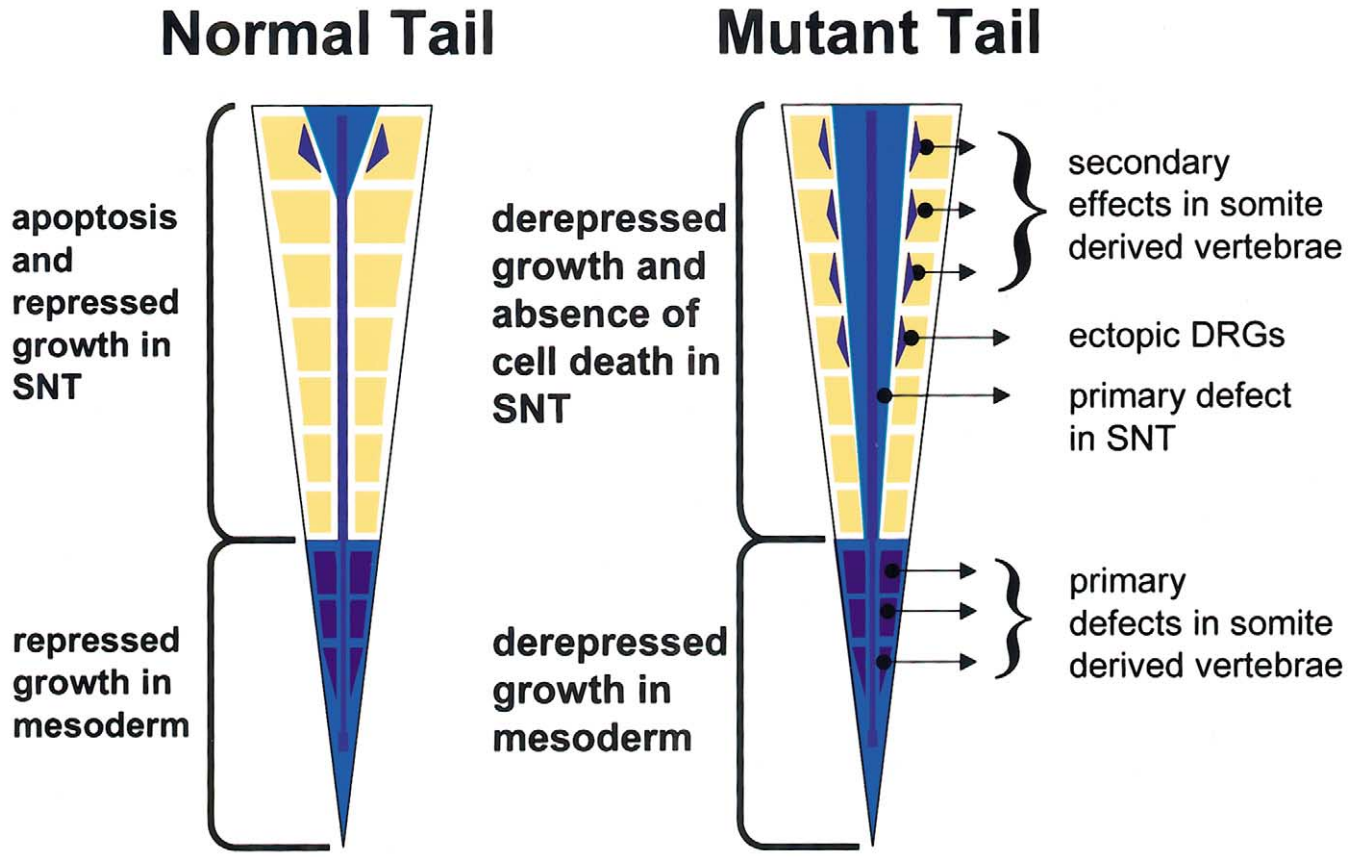

Fig. 8. Summary of expression of *Hoxb13* and associated phenotypes. A comparison of heterozygote and homozygous mutant expression patterns of *Hoxb13* in the developing tail at day 14.5 shows nonexpressing somites (yellow) and expressing somites and neural tubes (blue). All phenotypes in the adult can be explained by defects in proliferation and apoptosis within the *Hoxb13* expression domains in the developing embryo tail. Defects in *Hoxb13* nonexpressing domains, such as those seen in the bifid spinous processes of caudal vertebrae, are secondary to the enlarged spinal cord.

noted between *Hoxb13* homozygous mutants and controls is consistent with the later events that modify tail patterning.

Analogously to an overgrowth defect in the neural structures, homozygous mutants have larger caudal vertebrae in the most posterior one-third of the tail (cv 20–30). Larger caudal vertebrae are observed in the same region in which *Hoxb13* is expressed in the mesoderm during development. Overproliferation of cells in this region is the likely culprit for this phenotype since dorsal flexures appear at E12.5, which are frequently indicative of differences in cellular proliferation rates (Chen et al., 1994). The more rostral caudal vertebrae (cv 1–6) show changes in their structure where the vertebral foramena are larger and there is a greater distance between the spinous processes than in normal mice. These changes in structure are caused by the condensation of cartilage around a larger ectopic neural tube in the mutant. It is not likely that these are primary defects for the following two reasons; (1) *Hoxb13* expression is not detected in the mesoderm at the levels from which cv1–6 are derived; (2) these vertebrae do not show phenotypes characteristic of homeotic transformations in *Hox* gene mutants, such as presence or absence of spinous and transverse processes and the angles of transverse processes to the vertebral body. These are secondary defects and provide an illustration of how abnormal development of one structure can affect adjacent structures.

Hoxb13 in the peripheral nervous system

Disruption of *Hoxb13* appears to cause anterior homeotic transformations of the secondary neural tube and associated DRGs, such that the spinal cord is significantly longer and thicker and three to four ectopic DRGs are formed. At E13.5, these extra DRGs express *Hoxb13* just as the caudal-most DRGs do in heterozygotes. We believe that the function of *Hoxb13* in the SNT is to limit growth and proliferation of neural cells in the SNT both by activating apoptosis and by attenuating cell proliferation. A reduction of apoptotic cells in the SNT of mutant homozygotes and an increase in mitotic cells in the ventricular cell layer of the neural tube were consistently observed using TUNEL assays and pHH3 immunohistochemistry. More apoptotic cells can also be seen in the dorsal regions of the heterozygote tail on either side of the neural tube relative to ho-

mozygote tails, suggesting that neural crest cells that form the ectopic DRGs in homozygous mutants are normally removed by apoptosis.

It is interesting that axons in *Hoxb13* mutant homozygotes are defective in defasciculating from the segmental nerves. This phenotype provides evidence for an additional function of Hoxb13 in axon path finding. Supporting this hypothesis, *Hoxb13* is expressed in muscles that are adjacent to the segmental nerves. These muscle cells may provide a permissive or instructive cue for axons to leave the segmental nerve tracts and find targets in the periphery in a process similar to the role of muscle founder cells in axon defasciculation in *Drosophila* (Landgraf et al., 1999). If this is the case, *Hoxb13* may be partially redundant for this function since axons are not completely defective in this process and mice homozygous for the *Hoxb13* mutation still respond, though poorly, to external stimuli.

Evolutionary considerations

Vertebrate tails have evolved to perform many different functions in various taxa throughout the animal kingdom. Tails perform functions in balance, climbing, swinging, communication, and swimming. The diversity of tail functions is reflected in the diversity of tail patterns. For many vertebrates, such as *Lacertid* lizards and *Urodele* salamanders, evolution has established mechanisms by which these animals can jettison their tails in the event that they are attacked. Moreover, the proper tail length is so important that they have evolved tightly regulated mechanisms by which they can regenerate tail tissues after they are lost (Baranowitz et al., 1979).

Hoxb13 expression has been well characterized in developing and regenerating forelimbs, hindlimbs, and tail in the axolotl, *Ambystoma mexicanum*—a urodele salamander (Carlson et al., 2001). Urodeles are the only vertebrates that are known to be capable of regenerating limbs and tails as adults. Also, unlike higher vertebrates such as mice, urodele spinal cords span the entire length of their tails. In a regenerating neural tube, ependymal cells, which are types of radial glial cells, begin to proliferate in response to injury (Chernoff, 1996). *Hoxb13* has a similar expression pattern in the neural tube and surrounding mesenchyme of a developing axolotl tail as in a developing mouse tail. In an amputated embryonic axolotl tail, *Hoxb13* is first detected in the ependymal cells of the regenerating neural tube at approximately 3 days postamputation, followed by expression in the surrounding mesenchyme (Chernoff et al., 2002). Unlike in mice, however, axolotl *Hoxb13* is expressed in the developing axolotl hindlimb, and regenerating forelimbs and hindlimbs (Carlson et al., 2001).

The function of *Hoxb13* in axolotls is unknown. Although it may seem counterintuitive that at this stage of regeneration it would be prudent to turn on a gene that limits proliferation of cells, the timing of expression at 3 days postamputation in the tail may be consistent with a similar role for *Hoxb13* in axolotls as in mouse. The disparity in expression of *Hoxb13* between axolotl and mouse limbs may reflect the requirement to coordinate proliferation in a structure capable of regeneration such as the axoltl limb. This is consistent with the fact that in the axolotl forelimb *Hoxb13* expression has only been detected during regeneration and not during normal forelimb development (Carlson et al., 2001).

Hox genes typically function to assign cell fate and pattern embryonic structures. It has been proposed that *Hox* genes accomplish these tasks primarily by promoting proliferation of certain cell types (Duboule, 1995). This view has been supported by other work in the past. For example, in a transgenic approach in mice for another *Hox* gene, *Hoxc8*, increasing transgene dosage yielded the interesting result that higher levels of Hoxc8 kept chondrocytes in a proliferative state rather than allowing them to differentiate into prehypertrophic chondrocytes. The authors predict that higher concentrations of Hox transcription factors favor proliferation, while reduction stimulates differentiation of chondrocytes (Yueh et al., 1998). Similarly, experiments in the chick limb where *Hoxd13* and *Hoxd11* transgenes were misexpressed led to the proposal that all *Hox* genes promote growth but that some are more effective promoters of growth than others (Goff and Tabin, 1997). Our data suggest that, at least in the tail, *Hoxb13* has quite the opposite function. That is, *Hoxb13* limits proliferation and activates programmed cell death in the SNT and caudal-most somites. Although examples of *Hox* genes being involved in the activation of apoptotic pathways exist (Lohmann et al., 2002; Stadler et al., 2001), this is the first study to demonstrate a link between *Hox* gene expression and increased programmed cell death in vertebrate neural tissues. In contrast to the numerous descriptions of *Hox* mutants demonstrating increased apoptosis in neural tissues (Barrow et al., 2000; Gaufo et al., 2000; Rossel and Capecchi, 1999; Tiret et al., 1998), the hallmark of the loss-of-function of *Hoxb13* is decreased apoptosis.

The specific mechanisms involved in the inhibition of proliferation and activation of apoptotic pathways by Hoxb13, and whether these effects are or are not cell-autonomous, remain to be determined. In summary, however, we believe that *Hoxb13* expression heralds the end of both neural and somitic development in the embryo and find it interesting and appropriate that, while many *Hox* genes assign identity and promote growth along the anterior–posterior axis, *Hoxb13*, the most 5′ gene in the *HoxB* cluster, signals the repression of growth and activation of apoptosis in the caudal extremity of a developing embryo. Further study of *Hoxb13* and its downstream effects may provide insight to the mechanisms that repress neural proliferation and may lead to manipulations that overcome this repression.

Acknowledgments

We thank Nathaniel Heintz for the *Hoxb13* genomic construct and Marjorie Allen, Carol Lenz, Gail Peterson, and Sheila Barnett for ES cell culture work and blastocyst injection, and the vivarium staff for help with animal care. We also thank Gary Schoenwolf and members of the Capecchi laboratory for critical reading of the manuscript.

References

Asakura, A., Tapscott, S.J., 1998. Apoptosis of epaxial myotome in Danforth's short-tail (Sd) mice in somites that form following notochord degeneration. Dev. Biol. 203, 276–289.

Bachiller, D., Macias, A., Duboule, D., Morata, G., 1994. Conservation of a functional hierarchy between mammalian and insect Hox/HOM genes. EMBO J. 13, 1930–1941.

Baranowitz, S.A., Maderson, P.F., Connelly, T.G., 1979. Lizard and newt tail regeneration: a quantitative study. J. Exp. Zool. 210, 17–37.

Barrow, J.R., Stadler, H.S., Capecchi, M.R., 2000. Roles of Hoxa1 and Hoxa2 in patterning the early hindbrain of the mouse. Development 127, 933–944.

Carlson, M.R., Komine, Y., Bryant, S.V., Gardiner, D.M., 2001. Expression of Hoxb13 and Hoxc10 in developing and regenerating Axolotl limbs and tails. Dev. Biol. 229, 396–406.

Chen, W.H., Morriss-Kay, G.M., Copp, A.J., 1994. Prevention of spinal neural tube defects in the curly tail mouse mutant by a specific effect of retinoic acid. Dev. Dyn. 199, 93–102.

Chernoff, E., Sato, K., Corn, A., Karcavich, R., 2002. Spinal cord regeneration: intrinsic properties and emerging mechanisms. Semin. Cell. Dev. Biol. 13, 361.

Chernoff, E.A., 1996. Spinal cord regeneration: a phenomenon unique to urodeles? Int. J. Dev. Biol. 40, 823–831.

Chisaka, O., Capecchi, M.R., 1991. Regionally restricted developmental defects resulting from targeted disruption of the mouse homeobox gene hox-1.5. Nature 350, 473–479.

Condie, B.G., Capecchi, M.R., 1993. Mice homozygous for a targeted disruption of Hoxd-3 (Hox-4.1) exhibit anterior transformations of the first and second cervical vertebrae, the atlas and the axis. Development 119, 579–595.

Copp, A.J., Brook, F.A., 1989. Does lumbosacral spina bifida arise by failure of neural folding or by defective canalisation? J. Med. Genet. 26, 160–166.

Criley, B.B., 1969. Analysis of embryonic sources and mechanims of development of posterior levels of chick neural tubes. J. Morphol. 128, 465–501.

Davis, A.P., Witte, D.P., Hsieh-Li, H.M., Potter, S.S., Capecchi, M.R., 1995. Absence of radius and ulna in mice lacking hoxa-11 and hoxd-11. Nature 375, 791–795.

de Santa Barbara, P., Roberts, D.J., 2002. Tail gut endoderm and gut/genitourinary/tail development: a new tissue-specific role for Hoxa13. Development 129, 551–561.

Dolle, P., Dierich, A., LeMeur, M., Schimmang, T., Schuhbaur, B., Chambon, P., Duboule, D., 1993. Disruption of the Hoxd-13 gene induces localized heterochrony leading to mice with neotenic limbs. Cell 75, 431–441.

Duboule, D., 1995. Vertebrate Hox genes and proliferation: an alternative pathway to homeosis? Curr. Opin. Genet. Dev. 5, 525–528.

Duboule, D., Morata, G., 1994. Colinearity and functional hierarchy among genes of the homeotic complexes. Trends Genet. 10, 358–364.

Favier, B., Le Meur, M., Chambon, P., Dolle, P., 1995. Axial skeleton homeosis and forelimb malformations in Hoxd-11 mutant mice. Proc. Natl. Acad. Sci. USA 92, 310–314.

Favier, B., Rijli, F. M., Fromental-Ramain, C., Fraulob, V., Chambon, P., Dolle, P., 1996. Functional cooperation between the non-paralogous genes Hoxa-10 and Hoxd-11 in the developing forelimb and axial skeleton. Development 122, 449–460.

Fromental-Ramain, C., Warot, X., Lakkaraju, S., Favier, B., Haack, H., Birling, C., Dierich, A., Dolle, P., Chambon, P., 1996. Specific and redundant functions of the paralogous Hoxa-9 and Hoxd-9 genes in forelimb and axial skeleton patterning. Development 122, 461–472.

Gaufo, G.O., Flodby, P., Capecchi, M.R., 2000. Hoxb1 controls effectors of sonic hedgehog and Mash1 signaling pathways. Development 127, 5343–5354.

Goddard, J.M., Rossel, M., Manley, N.R., Capecchi, M.R., 1996. Mice with targeted disruption of Hoxb-1 fail to form the motor nucleus of the VIIth nerve. Development 122, 3217–3228.

Godwin, A.R., Capecchi, M.R., 1998. Hoxc13 mutant mice lack external hair. Genes Dev. 12, 11–20.

Goff, D.J., Tabin, C.J., 1997. Analysis of Hoxd-13 and Hoxd-11 misexpression in chick limb buds reveals that Hox genes affect both bone condensation and growth. Development 124, 627–636.

Gofflot, F., Hall, M., Morriss-Kay, G.M., 1997. Genetic patterning of the developing mouse tail at the time of posterior neuropore closure. Dev. Dyn. 210, 431–445.

Goldman, D.C., Martin, G.R., Tam, P.P., 2000. Fate and function of the ventral ectodermal ridge during mouse tail development. Development 127, 2113–2123.

Gruneberg, H., 1963. The Pathology of Development. Wiley, New York.

Gruneberg, H., Wickramaratne, G.A., 1974. A re-examination of two skeletal mutants of the mouse, vestigial-tail (vt) and congenital hydrocephalus (ch). J. Embryol. Exp. Morphol. 31, 207–222.

Keller-Peck, C.R., Mullen, R.J., 1997. Altered cell proliferation in the spinal cord of mouse neural tube mutants curly tail and Pax3 splotch-delayed. Brain Res. Dev. Brain Res. 102, 177–188.

Landgraf, M., Baylies, M., Bate, M., 1999. Muscle founder cells regulate defasciculation and targeting of motor axons in the Drosophila embryo. Curr. Biol. 9, 589–592.

Lohmann, I., McGinnis, N., Bodmer, M., McGinnis, W., 2002. The Drosophila Hox gene deformed sculpts head morphology via direct regulation of the apoptosis activator reaper. Cell 110, 457–466.

Lufkin, T., Mark, M., Hart, C.P., Dolle, P., LeMeur, M., Chambon, P., 1992. Homeotic transformation of the occipital bones of the skull by ectopic expression of a homeobox gene. Nature 359, 835–841.

Mansour, S.L., Goddard, J.M., Capecchi, M.R., 1993. Mice homozygous for a targeted disruption of the proto-oncogene int-2 have developmental defects in the tail and inner ear. Development 117, 13–28.

Mansour, S.L., Thomas, K.R., Capecchi, M.R., 1988. Disruption of the proto-oncogene int-2 in mouse embryo-derived stem cells: a general strategy for targeting mutations to non-selectable genes. Nature 336, 348–352.

Medina-Martinez, O., Bradley, A., Ramirez-Solis, R., 2000. A large targeted deletion of Hoxb1-Hoxb9 produces a series of single-segment anterior homeotic transformations. Dev. Biol. 222, 71–83.

Moody, S.A., Miller, V., Spanos, A., Frankfurter, A., 1996. Developmental expression of a neuron-specific beta-tubulin in frog (*Xenopus laevis*): a marker for growing axons during the embryonic period. J. Comp. Neurol. 364, 219–230.

Nievelstein, R.A., Hartwig, N.G., Vermeij-Keers, C., Valk, J., 1993. Embryonic development of the mammalian caudal neural tube. Teratology 48, 21–31.

O'Rahilly, R., Muller, F., Meyer, D.B., 1990. The human vertebral column at the end of the embryonic period proper. 4. The sacrococcygeal region. J. Anat. 168, 95–111.

Patterson, L.T., Pembaur, M., Potter, S.S., 2001. Hoxa11 and Hoxd11 regulate branching morphogenesis of the ureteric bud in the developing kidney. Development 128, 2153–2161.

Podlasek, C.A., Duboule, D., Bushman, W., 1997. Male accessory sex organ morphogenesis is altered by loss of function of Hoxd-13. Dev. Dyn. 208, 454–465.

Ramirez-Solis, R., Zheng, H., Whiting, J., Krumlauf, R., Bradley, A., 1993. Hoxb-4 (Hox-2.6) mutant mice show homeotic transformation of a cervical vertebra and defects in the closure of the sternal rudiments. Cell 73, 279–294.

Rossel, M., Capecchi, M.R., 1999. Mice mutant for both Hoxa1 and Hoxb1 show extensive remodeling of the hindbrain and defects in craniofacial development. Development 126, 5027–5040.

Schoenwolf, G.C., 1978. Effects of complete tail bud extirpation on early development of the posterior region of the chick embryo. Anat. Rec. 192, 289–295.

Schoenwolf, G.C., 1984. Histological and ultrastructural studies of secondary neurulation in mouse embryos. Am. J. Anat. 169, 361–376.

Schoenwolf, G.C., Chandler, N.B., Smith, J.L., 1985. Analysis of the origins and early fates of neural crest cells in caudal regions of avian embryos. Dev. Biol. 110, 467–479.

Schoenwolf, G.C., Delongo, J., 1980. Ultrastructure of secondary neurulation in the chick embryo. Am. J. Anat. 158, 43–63.

Schwenk, F., Baron, U., Rajewsky, K., 1995. A cre-transgenic mouse strain for the ubiquitous deletion of loxP-flanked gene segments including deletion in germ cells. Nucleic Acids Res. 23, 5080–5081.

Selby, P.B., 1987. A rapid method for preparing high quality alizarin stained skeletons of adult mice. Stain Technol. 62, 143–146.

Shum, A.S., Poon, L.L., Tang, W.W., Koide, T., Chan, B.W., Leung, Y.C., Shiroishi, T., Copp, A.J., 1999. Retinoic acid induces down-regulation of Wnt-3a, apoptosis and diversion of tail bud cells to a neural fate in the mouse embryo. Mech. Dev. 84, 17–30.

Stadler, H.S., Higgins, K.M., Capecchi, M.R., 2001. Loss of Eph-receptor expression correlates with loss of cell adhesion and chondrogenic capacity in Hoxa13 mutant limbs. Development 128, 4177–4188.

Studer, M., Gavalas, A., Marshall, H., Ariza-McNaughton, L., Rijli, F.M., Chambon, P., Krumlauf, R., 1998. Genetic interactions between Hoxa1 and Hoxb1 reveal new roles in regulation of early hindbrain patterning. Development 125, 1025–1036.

Studer, M., Popperl, H., Marshall, H., Kuroiwa, A., Krumlauf, R., 1994. Role of a conserved retinoic acid response element in rhombomere restriction of Hoxb-1. Science 265, 1728–1732.

Takada, S., Stark, K.L., Shea, M.J., Vassileva, G., McMahon, J.A., McMahon, A. P., 1994. Wnt-3a regulates somite and tailbud formation in the mouse embryo. Genes Dev. 8, 174–189.

Tiret, L., Le Mouellic, H., Maury, M., Brulet, P., 1998. Increased apoptosis of motoneurons and altered somatotopic maps in the brachial spinal cord of Hoxc-8-deficient mice. Development 125, 279–291.

van den Akker, E., Fromental-Ramain, C., de Graaff, W., Le Mouellic, H., Brulet, P., Chambon, P., Deschamps, J., 2001. Axial skeletal patterning in mice lacking all paralogous group 8 Hox genes. Development 128, 1911–1921.

van Straaten, H.W., Copp, A.J., 2001. Curly tail: a 50-year history of the mouse spina bifida model. Anat. Embryol. (Berl.) 203, 225–237.

van Straaten, H.W., Hekking, J.W., Copp, A.J., Bernfield, M., 1992. Deceleration and acceleration in the rate of posterior neuropore closure during neurulation in the curly tail (ct) mouse embryo. Anat. Embryol. (Berl) 185, 169–174.

Wellik, D.M., Hawkes, P.J., Capecchi, M.R., 2002. Hoxa1 paralogous genes are essential for metanephric kidney induction. Genes Dev. 16, 1423–1432.

Wittman, K.S., Krupa, P.L., Pesetsky, I., Hamburgh, M., 1972. Electron microscopy and histochemistry of tail regression in the brachyury mouse. Dev. Biol. 27, 419–424.

Yamaguchi, T.P., Takada, S., Yoshikawa, Y., Wu, N., McMahon, A.P., 1999. T (Brachyury) is a direct target of Wnt3a during paraxial mesoderm specification. Genes Dev. 13, 3185–3190.

Yoshikawa, Y., Fujimori, T., McMahon, A.P., Takada, S., 1997. Evidence that absence of Wnt-3a signaling promotes neuralization instead of paraxial mesoderm development in the mouse. Dev. Biol. 183, 234–242.

Yueh, Y. G., Gardner, D.P., Kappen, C., 1998. Evidence for regulation of cartilage differentiation by the homeobox gene Hoxc-8. Proc. Natl. Acad. Sci. USA 95, 9956–9961.

Zakany, J., Fromental-Ramain, C., Warot, X., Duboule, D., 1997. Regulation of number and size of digits by posterior Hox genes: a dose-dependent mechanism with potential evolutionary implications. Proc. Natl. Acad. Sci. USA 94, 13695–13700.

Zeltser, L., Desplan, C., Heintz, N., 1996. Hoxb-13: a new Hox gene in a distant region of the HOXB cluster maintains colinearity. Development 122, 2475–2484.